論文 / 著書情報
Article / Book Information

Title	Nonlinear dynamics of conduction electrons in organic conductors
Authors	TAKEHIKO MORI,Tatsuhiko Oozawa,Yoshimasa Bando,Tadashi Kawamoto,Shoichi Niizeki,Hatsumi Mori,Ichiro Terasaki
Citation	Phys. Rev. B, Vol. 79, No. 11,
発行日/Pub. date	2009, 3
公式URL/Journal URL	http://journals.aps.org/prb/
権利情報/Copyright	Copyright (c) 2009 American Physical Society

Nonlinear dynamics of conduction electrons in organic conductors

Takehiko Mori and Tatsuhiko Ozawa
Department of Chemistry and Materials Science, Tokyo Institute of Technology, O-okayama, Tokyo 152-8552, Japan

Yoshimasa Bando and Tadashi Kawamoto
Department of Organic and Polymeric Materials, Tokyo Institute of Technology, O-okayama, Tokyo 152-8552, Japan

Shoichi Niizeki and Hatsumi Mori
Institute for Solid State Physics, The University of Tokyo, Kashiwa 277-8551, Chiba

Ichiro Terasaki
Department of Applied Physics, Waseda University, Tokyo 169-8555, Japan

(Received 23 October 2008; revised manuscript received 8 February 2009; published 13 March 2009)

Nonlinear conductivity of organic conductors is explained quantitatively starting from a phenomenological energy-balance equation. Experimental results of $(TMET\text{-}TTP)_4PF_6$ are presented, where TMET-TTP is 2-[4, 5-bis(methylthio)-1,3-dithiol-2-ylidene]-5-[4,5-ethylenedithio-1,3-dithiol-2-ylidene]-1,3,4,6-tetrathiapentalene, and the simulation reproduces the nonlinear properties very well, including the voltage-current characteristics, power-law excess conductivity, and temperature dependence of the threshold field and current. The obtained heat capacity is much smaller than the lattice heat capacity, indicating unimportance of the Joule heating. Since the organic conductors show very little hysteretic switching, the time dependence of the energy balance is traced explicitly, defining nonlinear dynamics of hypothetical electron temperature, which reproduces oscillating states similar to that of the organic thyristor and even chaotic states under certain circumstances. It is expected that transient phenomena such as oscillatory and random outputs in some sort of organic and inorganic nonlinear conductors are quantitatively explained by this method, which in turn affords a playground of nonlinear dynamics.

DOI: 10.1103/PhysRevB.79.115108 PACS number(s): 72.80.Le, 72.20.Ht, 05.45.−a

I. INTRODUCTION

Nonlinear conductivity has long been investigated in a considerable number of materials, including inorganic semiconductors,[1,2] transition metal oxides,[3] low-dimensional materials,[4] and organic conductors,[5–9] and particular attention has been devoted to the potential application to switching and memory devices.[3,6] Recently, unusual spontaneous current oscillation, called an organic thyristor, has been found in the organic charge-transfer salt, θ-$(BEDT\text{-}TTF)_2CsZn(SCN)_4$ (BEDT-TTF: bis(ethylenedithio) tetrathiafulvalene),[8,9] followed by some other organic and inorganic materials, such as $K_{0.3}MoO_3$ and VO_2.[10–12] Giant nonlinear conductivity has been found in an increasing number of organic materials,[10,13–16] but there has been no sufficient framework to analyze nonlinear transport in organic conductors. Nonlinear transport in low-dimensional organic conductors has been investigated extensively on the basis of collective motion of density waves,[4] but this mechanism does not seem to apply to the recently found organic conductors. The nonlinear conductivity in the θ-phase organic conductor has been interpreted from the standpoint of competition between two charge-order patterns: a low-conducting stripe pattern and a high-conducting nonstripe pattern,[8,17] but we cannot quantitatively discuss the voltage-current *V-I* characteristics based on this mechanism. Takahide *et al.*[18,19] succeeded in explaining the power-law *V-I* characteristics at very low temperatures only assuming the long-range Coulomb interaction. For inorganic conductors, several theories of nonlinear transport have been proposed.[4,20–22] Among them, the electrothermal model is a phenomenological but classical standard approach that is useful to quantitatively discuss the *V-I* characteristics and the inhomogeneous current.[20] The present paper provides a macroscopic energy-balance analysis based on a modified thermal model that reproduces nonlinear transport and the oscillating phenomenon. Although the present analysis is generally applicable, we show comparison of observed and simulated nonlinear conductivities for a charge-transfer salt, $(TMET\text{-}TTP)_4PF_6$ (the molecular structure is depicted in Fig. 1) as an example to show the general analytic procedure. Since this compound shows a simple activated conductivity (Fig. 1),[23] the agreement between observation and simulation is particularly obvious. Although $(TMET\text{-}TTP)_4PF_6$ has a herringbonelike θ-type molecular arrangement as well, the composition is 4:1, and nonstripe charge order is the only expected charge-order phase, thus leading to the simple activated conductivity (Fig. 1).

When we slightly change an adjusting parameter from the actual one, we can reproduce oscillating states. The time-dependent energy-balance equation defines nonlinear dynamics of hypothetical electron temperature, represented by a single hump diagram just like the logistic map.[24] To analyze nonlinear conductivity, we can use mathematical methods that have been extensively studied in conjunction with nonlinear physics, chemical oscillations,[25] mathematical biology,[26] and social science.[27]

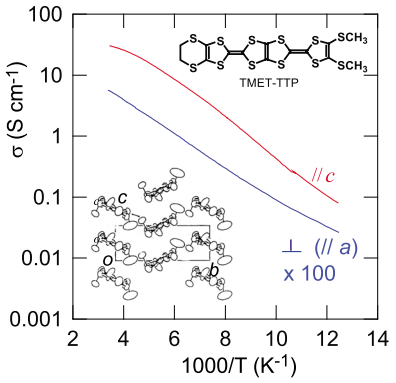

FIG. 1. (Color online) Temperature dependence of conductivity in $(TMET\text{-}TTP)_4PF_6$ with the molecular and crystal structures (Ref. 23). The conductivity is well represented by $\sigma=\sigma_1 \exp(-T_g/T)$, where $T_g=660$ K, $\sigma_1=450$ Ω cm for the in-plane conduction, and $\sigma_1=0.9$ Ω cm for the out-of-plane conduction.

II. EXPERIMENTAL

Single crystals of $(TMET\text{-}TTP)_4PF_6$ were prepared by electrochemical crystallization as described previously.[23] Nonlinear conductivity was measured with a short voltage or current pulse of 5 ms length and with a 1 s interval in order to avoid heating. Nonlinearity was observed when the electric fields were applied both along the crystallographic c (in-plane) and a (out-of-plane) axes. The sample cross section is $S=1.8\times10^{-5}$ cm^2, and the distance between the voltage contacts is $L=0.036$ cm for Fig. 2(a), $S=1.2\times10^{-5}$ cm^2 and $L=0.018$ cm for Fig. 2(b), and $S=9.6\times10^{-5}$ cm^2 and $L=0.002$ cm for Fig. 2(c).

III. RESULTS

Figure 2 compares observed and simulated nonlinear characteristics, plotted with respect to the current density J and the electric field E. We have carried out two different measurements: the four-probe and two-probe methods, hereafter abbreviated as 4P and 2P, respectively. In the 4P measurement, a regulated current pulse is applied to the outer two terminals, and voltage between the inner two terminals is measured [Fig. 2(a)]. Below 100 K, negative differential resistance (NDR) is observed. Although a variety of formulae that represent non-Ohmic conductivity has been proposed,[4,5] the present results seem to be well represented by a power-law phenomenological equation rather than the exponential dependence,[28]

$$\sigma(T,J) = \sigma_1 \exp(-T_g/T) + \sigma_2 J^m, \tag{1}$$

where the first term stands for the thermally activated Ohmic conductivity and the second term is current-dependent non-

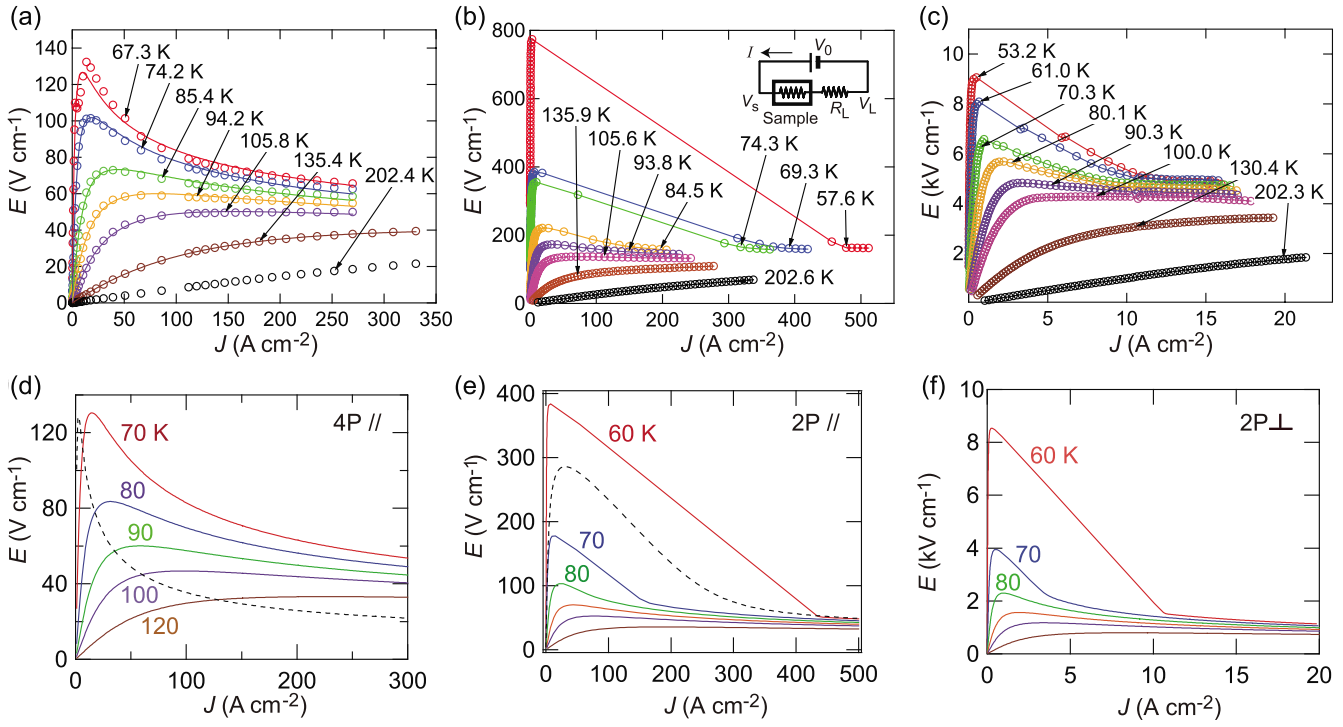

FIG. 2. (Color online) Observed (a)–(c) and simulated (d)–(f) nonlinear conductivities in $(TMET\text{-}TTP)_4PF_6$. (a) E-J characteristics measured by the four-probe method, applying a 5 ms current pulse parallel to the stacking direction ($\|c$). The fitting curves are derived from Eq. (1). (b) E-J characteristics measured by the two-probe method with application of a 5 ms voltage pulse parallel to the stacking direction ($\|c$). (c) E-J characteristics measured by the two-probe method with application of a voltage pulse perpendicular to the conducting sheet ($\|a$). (d) In-plane four-probe E-J characteristics simulated from Eq. (3) so as to reproduce (a). The dotted curve is based on smaller $\alpha=50$ W K^{-1} cm^{-3} at 60 K, and the other parameters are unchanged. (e) In-plane two-probe measurements at 60, 70, 80, 90, 100, and 120 K. $\rho_L=0.8$ Ω cm. The dotted curve is based on larger $nC=1.0$ J K^{-1} cm^{-3} at 70 K. (f) Out-of-plane two-probe measurements ($\|a$) at 60, 70, 80, 90, 100, and 120 K. $\rho_L=860$ Ω cm.

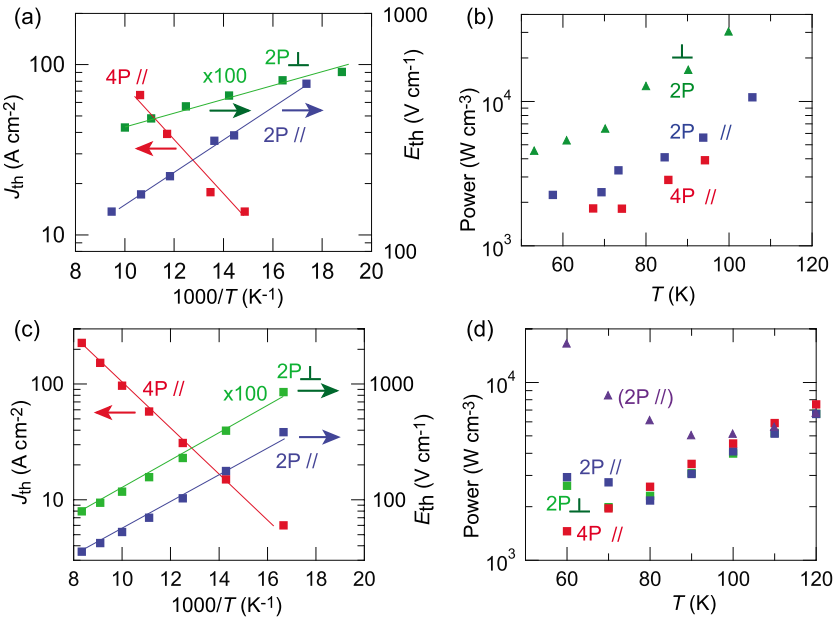

FIG. 3. (Color online) Temperature dependence of observed and simulated threshold currents, fields, and power in $(TMET\text{-}TTP)_4PF_6$. (a) Observed temperature dependence of J_{th} extracted from Fig. 2(a) and of E_{th} from Figs. 2(b) and 2(c). (b) Observed temperature dependence of the applied power $J_{th} \times E_{th}$ at the threshold, taken from Figs. 2(a)–2(c). (c) Simulated J_{th} taken from Fig. 2(d), and E_{th} from Figs. 2(e) and 2(f). (d) Simulated threshold power taken from Figs. 2(d)–2(f). The triangles are based on larger $nC=1.0$ J K^{-1} cm^{-3}.

linear conductivity. Though the microscopic basis of this equation is not certain, many compounds follow this equation, where the exponent is usually about $m=1.5$.[10,28] The NDR region in Fig. 2(a) follows a power law with $m=1.28$. The temperature dependence of the threshold current J_{th}, extracted from the peaks in Fig. 2(a), is plotted in Fig. 3(a). The threshold current is represented by an activated process $J_{th} \propto \exp(-T_a/T)$ with the activation energy of $T_a=380$ K.

In the 2P measurement, a voltage pulse (V_0) is applied to the circuit shown in the inset of Fig. 2(b). A sample electric field $E=V_s/L$ is calculated from the sample voltage $V_s=V_0-R_LI$, where $R_L=5$ kΩ is series load resistance and I is the measured current. Figures 2(b) and 2(c) show the 2P measurements in the in-plane ($\|c$) and out-of-plane ($\|a$) directions. The E-J characteristics show remarkable NDR. In contrast to inorganic thin films, no hysteresis or switching effects have been observed when V_0 decreases. The threshold electric fields E_{th}, extracted from the peaks, are plotted in Fig. 3(a). E_{th} is well represented by an activated process $E_{th} \propto \exp(T_a/T)$ with the activation energy of $T_a=220$ K ($\|c$) and 400 K ($\|a$). The threshold power increases with increasing the temperature [Fig. 3(b)].

IV. SIMULATION

When nonlinear transport originates in definite collective mode such as charge density waves, we can investigate the detail starting from the corresponding equation of motion.[4] Since this is not possible in the present case, we have to develop a phenomenological model on the basis of macroscopic quantities. It is customary in device physics to discuss high-field transport from the standpoint of hot electrons,[29] postulating that they follow the energy conservation.[1,2,20]

$$nC\frac{dT_e}{dt} = P + \nabla \cdot (K \nabla T_e). \tag{2}$$

The supplied energy is $P=\sigma(T_e)E^2$ for the voltage-regulated 2P measurement and $P=J^2/\sigma(T_e)$ for the current-regulated 4P measurement. This P term gives rise to the energy gain of the electrons, and increases electron temperature T_e as estimated from the left-hand side (C term). C corresponds to electron heat capacity per carrier and n is the carrier number density so that nC is the electron heat capacity per volume. The last K term gives the spatial distribution of T_e due to thermal conductivity K. The resulting filamentary current has usually been investigated in a steady state by neglecting the C term.[20] Since filamentary current is relatively unimportant in the present elongated samples, we explicitly deal with the C term instead, and the K term is simplified to the Newtonian cooling $-\alpha(T_e-T)$, where T refers to the environmental temperature and α stands for the energy transfer rate from the electron system to the lattice. α may change depending on the sample shape and the surface area. Accordingly, the energy-balance equation is, for the current-regulated 4P measurement,

$$nC\frac{dT_e}{dt} = J^2/\sigma(T_e) - \alpha(T_e - T). \tag{3}$$

This is valid for homogeneous or constant T_e distribution under certain boundary conditions.

In conventional inorganic semiconductors, such as GaAs, mobility drops at high fields. In the present case, however, the conductivity increases both at high fields and at high temperatures so that high-field conductivity $\sigma(T_e)$ is represented by the corresponding low-current conductivity taken from Fig. 1 at T_e, elevated from the environmental temperature T. Although we do not necessarily intend to attribute the nonlinearity to thermal effects, T_e is uniquely defined from σ and represents the population of the excited states rather than the thermal equilibrium so that the real lattice temperature T_L can be different from T_e.[30] It should be emphasized that although the present formulation is identical to the classical thermal model,[20] the hypothetical electron temperature T_e is not a real temperature but a parameter characterizing the population of the excited states. Then T_L rather than T_e cor-

responds to the electron temperature in the classical electrothermal model,[20] where the difference of resistances at T_L and T_e is attributed to the high electric field. Nevertheless, the present formulation largely simplifies the following nonlinear dynamics.

To numerically calculate Eq. (3), we take T_e at discrete times. First we calculate the right-hand side and estimate the rise in T_e from the left-hand side. Then, the new T_e is used to estimate the next right-hand side $\sigma(T_e)$ and $\alpha(T_e-T)$, and this process is repeated. By taking one step to be 0.1 ms, we carried out 50 iterations to reproduce a 5 ms pulse.

Simulated characteristics are shown in Figs. 2(d)–2(f). Figure 2(d) represents the 4P E-J characteristics, which correspond to the observation in Fig. 2(a). Figures 2(e) and 2(f) show the 2P characteristics corresponding to Figs. 2(b) and 2(c). The simulations look very similar to the experiments. Once $\sigma(T_e)$ is determined (Fig. 1), there are only two parameters, C and α, which are adjusted so as to reproduce the observed E-J curves. The parameters used are $nC=0.1$ J K^{-1} cm^{-3} and $\alpha=200$ W K^{-1} cm^{-3} throughout the present paper unless otherwise stated.

From these simulations, $J_{\rm th}$ and $E_{\rm th}$ are extracted as shown in Fig. 3(c). The results satisfactorily reproduce the experiments [Fig. 3(a)]. The activation energies are 440 ($4P\|c$), 300 ($2P\|c$), and 300 K ($2P\|a$). The simulation verifies the relations such as $J_{\rm th}\propto\exp(-T_a/T)$ and $E_{\rm th}\propto\exp(T_a/T)$. In the low-current limit, it is instructive to neglect the K term in Eq. (3) because T_e is very close to T;

$$P=\sigma E^2=nC\frac{\Delta T_e}{\tau}, \tag{4}$$

where T_e rises by ΔT_e after the time of τ. If this relation is valid up to the threshold $E_{\rm th}$ while σ is kept unchanged, $E_{\rm th}$ is obtained as $E_{\rm th}=(nC\frac{\Delta T_e}{\tau\sigma})^{1/2}$. Since P is J^2/σ in the current-regulating 4P measurement, $J_{\rm th}$ is $J_{\rm th}=(nC\frac{\Delta T_e}{\tau}\sigma)^{1/2}$. These equations demonstrate that $E_{\rm th}$ is proportional to $\sigma^{-1/2}$, whereas $J_{\rm th}$ is proportional to $\sigma^{1/2}$. This is the reason why $E_{\rm th}$ *increases* at low temperatures, while $J_{\rm th}$ *decreases*.

This simple approximation indicates that if σ follows an activated process with an activation energy of T_g, activation energies of $E_{\rm th}$ and $J_{\rm th}$ are both afforded by $T_a=T_g/2$. The observations are 220 K for $E_{\rm th}$ and 380 K for $J_{\rm th}$, and the sum (600 K) is approximately equal to $T_g=660$ K. The experiments as well as the simulation show that T_a for $E_{\rm th}$ is smaller than that for $J_{\rm th}$. As a consequence, the threshold power $J_{\rm th}\times E_{\rm th}$ increases as the temperature rises [Fig. 3(d)].

In 4P measurement, a constant current pulse is applied, and the voltage (E) behaves as shown in Fig. 4(a). First the resistance is high and very high voltage is applied. As a result, T_e and σ increase. Accordingly, the voltage drops until equilibrium is reached after about 0.5 ms. As shown in Fig. 4(b), the P term drops and the K term increases. After 0.5 ms, the P term equals the K term, and the C term disappears. T_e does not increase further, and the system is in equilibrium. By varying the applied J, the equilibrium T_e and the P term are depicted in Fig. 4(c). The P term equals the K term and is exactly proportional to T_e-T.

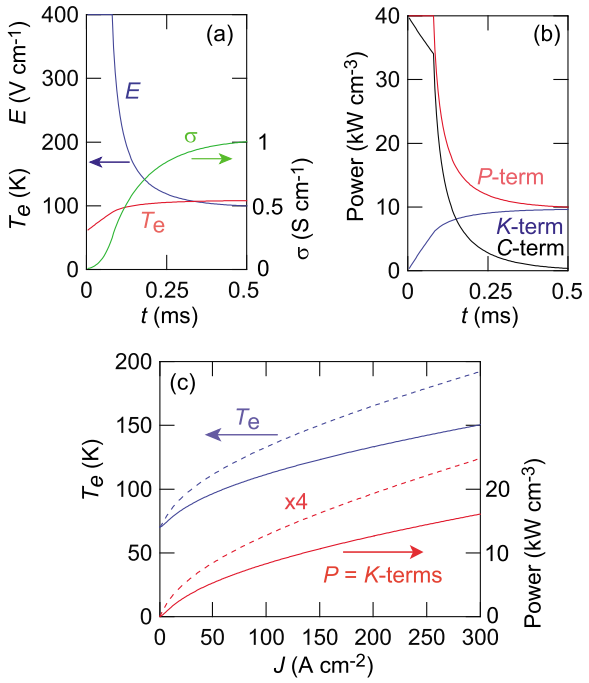

FIG. 4. (Color online) (a) Time profile in 4P measurement, E, σ, and T_e; and (b) P term, K term, and C term in Eq. (3) at $J=100$ A cm^{-2} and $T=60$ K. (c) J dependence of equilibrium T_e and the P term at 70 K. The solid curves are for $\alpha=200$ W K^{-1} cm^{-3} and the dotted ones for $\alpha=50$ W K^{-1} cm^{-3}.

If the pulse is too short to reach equilibrium, the E-J curve deviates from the calculation. Since this does not happen in the actual observations, equilibrium is achieved. This also indicates the absence of filamentary current in the 4P characteristics because it leads to highly conducting ON states, which should bifurcate from the homogeneous curve.[20]

In this calculation, we have limited the maximum applied field to 400 V cm^{-1}, as the actual current source does. Otherwise, on account of the initial high resistance state, the initial voltage becomes very large, exceeding 1000 V, and results in overshooting T_e. The very high T_e gradually drops to the equilibrium value, but it takes a longer time.

For another plot of the E-J curves, Fig. 5(a) shows the ρ-J curves. The flat low-current region indicates an Ohmic characteristic, and the resistivity drops following the J power, where the resistivity is represented by Eq. (1) with $m=1.40$. As a simple approximation to the high-current limit, the C term is neglected in an equilibrium state; Eq. (3) gives $E=\frac{\alpha(T_e-T)}{J}$, and E is inversely proportional to J for the constant K term. This represents NDR, leading to $\sigma\propto J^2$. The actual m is smaller than this because T_e increases at high currents.

As an improved approximation, Eq. (3) gives an implicit function, $J^2/\sigma(T_e)=\alpha(T_e-T)$. This function does not depend on C. By systematically varying α, the peak height of the E-J curve [Fig. 2(d)], corresponding to $E_{\rm th}$, is plotted in Fig. 5(b), together with the exponent m. As α decreases, heat dissipation decreases and the equilibrium T_e rises [dotted curves in Fig. 4(c)]. This leads to relatively low resistance at high currents, and the right end of the E-J curve falls, as exemplified by the dotted curve in Fig. 2(d). For the same

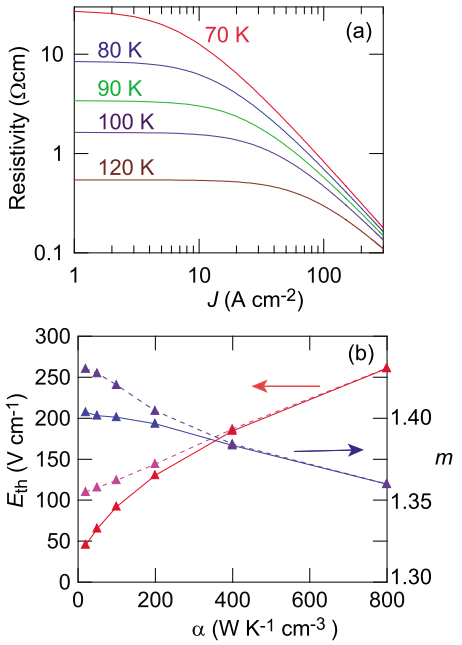

FIG. 5. (Color online) (a) ρ-J plot of the 4P measurement. (b) α dependence of the peak height $E_{\rm th}$ in Fig. 2(d) and m in Eq. (1) at 70 K. The solid curves are for nC=0.1 J K^{-1} cm^{-3}, and the dotted curves for nC=1.0 J K^{-1} cm^{-3}.

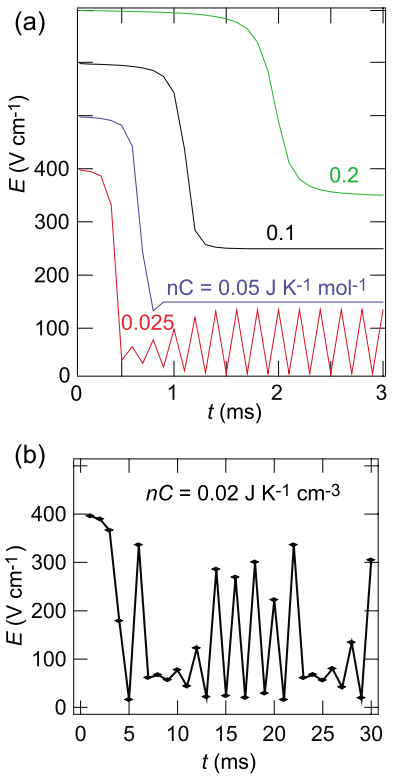

FIG. 6. (Color online) (a) Simulated time profile of a voltage pulse in 2P measurement with various electron heat capacities. The vertical axis was shifted appropriately. (b) Chaos appears at nC =0.02 J K^{-1} cm^{-3}.

reason, $E_{\rm th}$ decreases and m increases in Fig. 5(b). In particular, $E_{\rm th}$ is a sensitive function of α, and comparing $E_{\rm th}$ with the actual observation [Fig. 2(a)], we can determine α to be 200 W K^{-1} cm^{-3}.

In the 2P measurements, it is characteristic that the peak tops in Figs. 2(b) and 2(c) are located very close to the vertical axis. This indicates that the power at the threshold is relatively small. A large C gives rise to a round threshold peak, as exemplified in Fig. 2(e). In the transient state, as shown in Fig. 6(a), at the beginning most voltage is applied to the sample, but then it abruptly drops. The delay time is proportional to C. To reproduce the observed sharp threshold peaks and delay times, we have chosen nC =0.1 J K^{-1} cm^{-3}.

As shown in the triangles in Fig. 3(d), large C makes the threshold power large. In order to reproduce the observed small threshold power, we have to choose nC =0.1 J K^{-1} cm^{-3}. In another interpretation, from Eq. (4) the delay time τ is proportional to C. Thus, τ gives a good measure of C. The delay time in Fig. 6(a), together with the threshold power in Fig. 3(d), provides that the transition takes place at ΔT_e as small as 1 K. This is applied to the actual threshold power [Fig. 3(b)] to give nC =0.1 J K^{-1} cm^{-3} again.

In the actual system, C should be temperature dependent; electronic C is T linear, and lattice C is proportional to T^3. We have carried out a simulation by assuming temperature-dependent C, but, as shown in Fig. 4(d), even a constant C gives T-dependent power, and we could not find clear evidence that we have to assume a T-dependent C. This comes in part from the fact that the 4P measurement is essentially independent of C.

The above value nC=0.1 J K^{-1} cm^{-3} affords C =33.7 J K^{-1} mol^{-1}/molecule because n is inverse of the lattice volume per carrier (per four molecules),[20] $V_{\rm cell}$ =1348 cm^3 mol^{-1}, derived from the lattice volume, 2240 Å^3. Although the lattice heat capacity of organic conductors at around 60 K is ambiguous, it is approximately 300 J K^{-1} mol^{-1} per two molecules, based on a smaller molecule.[16,31] Per four molecules, this number should be doubled. Furthermore, the present large TMET-TTP molecule includes nearly twice the number of atoms, and should have nearly twice-larger heat capacity: approximately 1200 J K^{-1} mol^{-1} per four molecules or 300 J K^{-1} mol^{-1} per molecule. Consequently, the obtained C is an order of magnitude smaller than the expected lattice heat capacity.

The small C may be attributable to the inhomogeneous high-conducting state.[32] If the high-conducting path is one-tenth of the total volume, it may be reasonable to assume that the observed C is one-tenth of the total C. The influence of the filamentary current can be included in the small C.[20] In another interpretation, if we consider T_L independent of T_e (Fig. 7), we assume the energy conservation for the lattice.

$$nC_L\frac{dT_L}{dt} = \alpha_e(T_e - T_L) - \alpha_L(T_L - T). \tag{5}$$

The first term in the right-hand side is the input energy from the electron system, and the second term is the outgoing energy. In a steady state, the left-hand side is zero, and

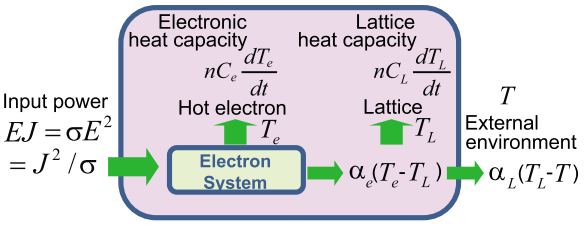

FIG. 7. (Color online) Schematic representation of energy flow from the electron system to the lattice and to the external environment.

$$\frac{T_L - T}{T_e - T_L} = \frac{\alpha_e}{\alpha_L}. \tag{6}$$

Here the overall C_a is the weighted average of the electron and lattice.

$$C_a = C_e + \frac{T_L - T}{T_e - T} C_L \tag{7}$$

because the energy values required to heat the electron and lattice are $C_e(T_e - T)$ and $C_L(T_L - T)$, respectively. Accordingly, $C_a/C_L = 1/10$ indicates $\frac{T_L - T}{T_e - T_L} = 1/10$, and $\alpha_e/\alpha_L = 1/10$. α_L is 10 times larger than α_e, and T_L remains still close to T in the $\alpha_e \ll \alpha_L$ limit. For example, the high-current end of Fig. 4(c) affords $T_e = 150$ K for $T = 70$ K, but the lattice temperature remains $T_L = 80$ K. C_a/C_L should be estimated for individual compounds, but similar ratios have been obtained for other organic compounds.

V. NONLINEAR DYNAMICS

In Eq. (3), the C and K terms are linear with respect to T_e, but the P term is nonlinear. As we did in the iterative calculation, the left-hand side gives ΔT_e and determines new T_e, leading to the successive development of T_e. Accordingly, this equation defines nonlinear dynamics with respect to T_e. Figure 8(a) plots ΔT_e in the vertical axis given by T_e plotted in the horizontal axis. In the 4P measurement, the curve crosses zero at point A. When T_e is lower than A, positive ΔT_e increases T_e to approach A. Above A, ΔT_e is negative and T_e decreases to approach A. Therefore, A is a stable fixed point.

For the 2P measurement without R_L, in Eq. (3), $J^2/\sigma(T_e)$ is simply replaced by $E^2\sigma(T_e)$. As shown in Fig. 8(a), the resulting curve crosses zero at B from negative to positive. Below B, T_e decreases to zero, whereas above B, T_e increases to infinity. Accordingly, B is an unstable bifurcation point. When we insert a load resistor, Eq. (3) changes to

$$nC\frac{dT_e}{dt} = (E_0 - \rho_L J)^2 \sigma(T_e) - \alpha(T_e - T) \tag{8}$$

and the curve becomes that shown in Fig. 8(b). This is a return map in which the vertical axis is $T_e + \Delta T_e$ instead of ΔT_e.[33] The curve crosses the slope=1 line at C. A point starting from D approaches C and E approaches C so that C is a stable point. When sufficiently low voltage is applied ($E_0 = 100$ V/cm), the resulting green curve is located below the slope=1 line, and the low-conducting state at $T_e = T$ is the stable point.

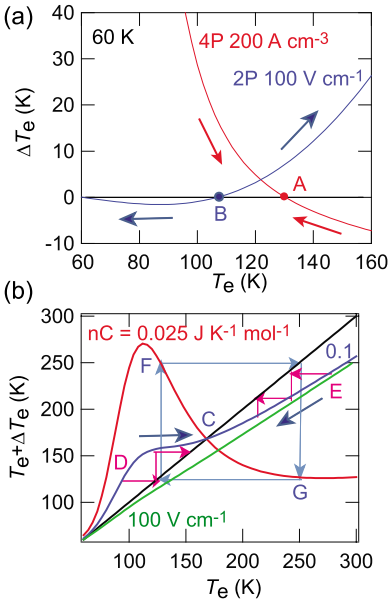

FIG. 8. (Color online) (a) ΔT_e given by T_e for 4P (red curve at $J = 200$ A cm^{-2}) and 2P (blue curve at $E = 100$ V cm^{-1}) measurements at 60 K and $nC = 0.1$ J K^{-1} cm^{-3}. (b) Return map, where $\Delta T_e + T_e$ is given by T_e for 2P measurement with a load resistor $\rho_L = 0.8$ Ω cm at $T = 60$ K. Blue ($E_0 = 400$ V cm^{-1}) and green ($E_0 = 100$ V cm^{-1}) curves at $nC = 0.1$ J K^{-1} cm^{-3}, and red curve ($E_0 = 400$ V cm^{-1}) at $nC = 0.025$ J K^{-1} cm^{-3}.

If we use an artificially small nC, the hump is more pronounced, and the point starting from F goes to G and oscillates around C. This is why oscillation occurs in Fig. 6(a) (red curve). Accordingly, the observation of oscillation is strong evidence of small nC and of only a small contribution of lattice heating. In the oscillating state, T_e takes two values alternately. The frequency can be discussed by incorporating a parameter characterizing the delay in Eq. (8).[26] Equation (8) is different from the conventional nonlinear circuit using an NDR device because it does not contain a term coming from a capacitor. The present oscillation is an inherent property of the material.

The return map is a single hump diagram analogous to the logistic map,[24] and chaos appears for smaller nC [Fig. 6(b)], where no more periodicity is observed. We have observed analogous random output in conditions similar to those of the spontaneous current oscillation. The present model can explain the wide band noise and random oscillation, which have been frequently observed together with nonlinear transport.[4,34–36]

The bifurcation diagram plotted for $(nC)^{-1}$ is depicted in Fig. 9. Only one stable point appears for $(nC)^{-1} < 37.8$ K cm^3 J^{-1}, and the present material [$(nC)^{-1} = 10$ K cm^3 J^{-1}] is located in this region. Above this, period two oscillation occurs. It bifurcates to period four at 47.2, and chaos appears for larger values. Period three appears at around 51.4. The diagram is relevant up to 62.4.

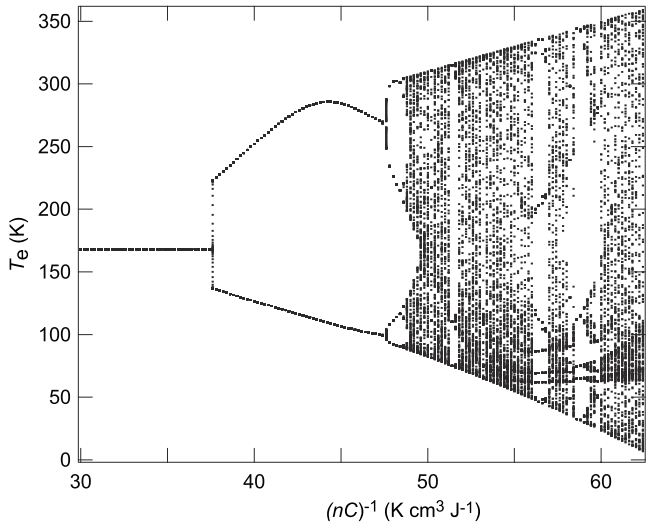

FIG. 9. Bifurcation diagram at E_0=400 V cm^{-1} and T=60 K.

VI. CONCLUSION

In conclusion, we have demonstrated that many features of nonlinear conductivity are understood from the standpoint of nonlinear dynamics with respect to T_e. The E-J characteristics, the power-law current dependence of the excess conductivity, and the activated temperature dependence of $E_{\rm th}$ and $J_{\rm th}$ are derived from this model. The 4P characteristics, as well as the low-conductive and high-conductive states in the 2P measurements, are respectively equilibrium states and have been dealt with in the steady state.[20] The present investigation demonstrates that the explicit evaluation of the time-dependent C term defines nonlinear dynamics and leads to oscillation and chaos inherent in the nonlinear transport.

We have applied similar simulations to other nonlinear organic materials and obtained basically similar results.[9,10] The obtained results are, however, very sensitive to the functional shape of $\sigma(T_e)$. Since $\sigma(T_e)$ of these compounds does not behave in a simple activated manner, more detailed analysis is necessary to attain quantitative agreement. On the other hand, unusual two-step E-J characteristics have been observed in another organic compound.[16] A variety of $\sigma(T_e)$, not limited to organics, is expected to afford a playground of nonlinear dynamics.

We have started from a simple formulation that is basically the same as the thermal model, but the obtained small C indicates that the simple thermal model is inappropriate. Accordingly, T_e is an abstract parameter that characterizes the excited states rather than the real sample temperature. Nonetheless, the present method provides a simple way to analyze the nonlinear characteristics and the time dependence quantitatively. There have been several attempts to analyze the chaotic outputs associated with nonlinear transport as nonlinear time series,[37,38] but the nonlinear dynamics behind them has not been described. The present approach potentially provides a way to construct a nonlinear model that can explain the oscillating and random outputs.

ACKNOWLEDGMENTS

This work is financially supported in part by a Grant-in-Aid for Scientific Research (B) (Contract No. 17340114), for Young Scientists (B) (Contract No. 17750176), and on Priority Areas of Molecular Conductors (Contract No. 15073211) from MEXT, Japan.

[1] E. M. Conwell, Solid State Phys. **S9**, 81 (1967).
[2] P. Stratton, Prog. Dielectr. **3**, 235 (1961).
[3] S. Q. Liu, N. J. Wu, and A. Ignatiev, Appl. Phys. Lett. **76**, 2749 (2000).
[4] G. Grüner, *Density Waves in Solids* (Addison-Wesley, Reading, MA, 1994).
[5] Y. Tokura, H. Okamoto, T. Koda, T. Mitani, and G. Saito, Phys. Rev. B **38**, 2215 (1988).
[6] T. Mori and K. Kawamoto, Annu. Rep. Prog. Chem., Sect. C: Phys. Chem. **103**, 134 (2007).
[7] T. Mori, H. Mori, and I. Terasaki, J. Mater. Chem. **17**, 4343 (2007).
[8] F. Sawano, I. Terasaki, H. Mori, T. Mori, M. Watanabe, N. Ikeda, Y. Nogami, and Y. Noda, Nature (London) **437**, 522 (2005).
[9] K. Inagaki, I. Terasaki, H. Mori, and T. Mori, J. Phys. Soc. Jpn. **73**, 3364 (2004).
[10] T. Mori, Y. Bando, T. Kawamoto, I. Terasaki, K. Takimiya, and T. Otsubo, Phys. Rev. Lett. **100**, 037001 (2008).
[11] A. Maeda, M. Notomi, K. Uchinokura, and S. Tanaka, Phys. Rev. B **36**, 7709 (1987).
[12] Y. W. Lee, B.-J. Kim, J.-W. Lim, S. J. Yun, S. Choi, B.-G. Chae, G. Kim, and H.-T. Kim, Appl. Phys. Lett. **92**, 162903 (2008).
[13] H. Endo, T. Kawamoto, T. Mori, I. Terasaki, T. Kakiuchi, H. Sawa, M. Kodani, K. Takimiya, and T. Otsubo, J. Am. Chem. Soc. **128**, 9006 (2006).
[14] T. Mori, T. Kawamoto, I. Terasaki, T. Kakiuchi, and H. Sawa, Phys. Rev. B **75**, 235103 (2007).
[15] R. Kondo, M. Higa, and S. Kagoshima, J. Phys. Soc. Jpn. **76**, 033703 (2007).
[16] S. Niizeki, F. Yoshikane, K. Kohno, K. Takahashi, H. Mori, Y. Bando, T. Kawamoto, and T. Mori, J. Phys. Soc. Jpn. **77**, 073710 (2008).
[17] T. Mori, J. Phys. Soc. Jpn. **72**, 1469 (2003).
[18] Y. Takahide, T. Konoike, K. Enomoto, M. Nishimura, T. Terashima, S. Uji, and H. M. Yamamoto, Phys. Rev. Lett. **96**, 136602 (2006).
[19] Y. Takahide, T. Konoike, K. Enomoto, M. Nishimura, T. Terashima, S. Uji, and H. M. Yamamoto, Phys. Rev. Lett. **98**, 116602 (2007).
[20] D. M. Kroll, Phys. Rev. B **9**, 1669 (1974).
[21] T. Oka, R. Arita, and H. Aoki, Phys. Rev. Lett. **91**, 066406 (2003).
[22] A. Maeda, Y. Inoue, H. Kitano, S. Savel'ev, S. Okayasu, I. Tsukada, and F. Nori, Phys. Rev. Lett. **94**, 077001 (2005).

[23] T. Mori, H. Inokuchi, Y. Misaki, H. Nishikawa, T. Yamabe, H. Mori, and S. Tanaka, Chem. Lett. **22**, 733 (1993).
[24] R. M. May, Nature (London) **261**, 459 (1976).
[25] P. Gray and S. K. Scott, *Chemical Oscillations and Instabilities* (Clarendon, Oxford, 1990).
[26] F. Brauer and C. Castillo-Chavez, *Mathematical Models in Population Biology and Epidemiology* (Springer, Berlin, 2000).
[27] C. Grebogi and J. A. Yorke, *The Impact of Chaos on Science and Society* (United Nations University Press, Tokyo, 1997).
[28] Y. Iwasa, T. Koda, S. Koshihara, Y. Tokura, N. Iwasawa, and G. Saito, Phys. Rev. B **39**, 10441 (1989).
[29] S. M. Sze, *Physics of Semiconductor Devices*, 2nd ed. (Wiley, New York, 1981), p. 645.
[30] H. Jain and A. K. Raychaudhuri, Appl. Phys. Lett. **93**, 182110 (2008).
[31] K. Saito, A. Sato, K. Kikuchi, H. Nishikawa, I. Ikemoto, and M. Sorai, J. Phys. Soc. Jpn. **69**, 3602 (2000).
[32] Y. Okimoto, R. Kumai, E. Saitoh, M. Izumi, S. Horiuchi, and Y. Tokura, Phys. Rev. B **70**, 115104 (2004).
[33] R. L. Devaney, *A First Course in Chaotic Dynamical Systems: Theory and Experiments* (Perseus, Cambridge, MA, 1992).
[34] A. Maeda, M. Notomi, and K. Uchinokura, Phys. Rev. B **42**, 3290 (1990).
[35] T. Bohr, P. Bak, and M. H. Jensen, Phys. Rev. A **30**, 1970 (1984).
[36] A. Zettl and G. Grüner, Comments Condens. Matter Phys. **12**, 265 (1986).
[37] S. Martin, H. Leber, and W. Martienssen, Phys. Rev. Lett. **53**, 303 (1984).
[38] Ch. Karakotsou, A. N. Anagnostopoulos, K. Kambas, and J. Spyridelis, Phys. Rev. B **46**, 16144 (1992).